JOURNAL OF THE KOREAN ASTRONOMICAL SOCIETY
34: 17~24, 2001

STUDY OF M82 USING SPECTRA FROM THE INFRARED SPACE OBSERVATORY

JUNGJOO SOHN[1,2,3], H. B. ANN[1], SOOJONG PAK[2], AND H. M. LEE[2,3]
[1]Department of Earth Science, Pusan National University
[2]Astronomy Program, School of Earth and Environmental Sciences, Seoul National University
[3]Infrared Astrophysics Group, Institute of Space and Astronautical Science, Japan
Email: jjsohn@astro.snu.ac.kr
(Received Feb. 20, 2001; Accepted Mar. 12, 2001)

ABSTRACT

We have studied the central parts of M82, which is a well-known infrared luminous, starburst galaxy, by analyzing archival data from the Infrared Space Observatory (ISO). M82 was observed at 11 positions covering ±45" from the center along the major axis. We analyzed 4 emission lines, [ArIII] 8.99 μm, H_2 17.034 μm, [FeII] 25.98 μm, and [SiII] 34.815 μm from SWS02 data. The integrated flux distributions of these lines are quite different. The H_2 line shows symmetric twin peaks at ~18" from the center, which is a general characteristic of molecular lines in starburst or barred galaxies. This line appears to be associated with the rotating molecular ring at around ~200 pc just outside the inner spiral arm. The relative depletion of the H_2 line at the center may be due to the active star formation activity which dissociates the H_2 molecules. The other lines have peaks at the center and the distributions are nearly symmetric. The line profiles are deconvolved assuming that both intrinsic and instrumental profiles are Gaussian. The velocity dispersion outside the core is found to be ~50 km s^{-1}. The central velocity dispersion is much higher than 50 km s^{-1}, and different lines give different values. The large central velocity dispersion (σ) is mostly due to the rotation, but there is also evidence for a high σ for [ArIII] line. We also generated position-velocity maps for these four lines. We found very diverse features from these maps.

Key words: galaxies: starburst galaxies, individual (M82) – methods: data analysis

I. INTRODUCTION

The Infrared Space Observatory (ISO: Kessler et al. 1996) was able to carry out both spectroscopic and photometric observations for a limited number of selected sources. It was operated for 28 months from November 1995 to April 1998 with a wide wavelength coverage (2.4-240 μm) and various instruments. The data in the ISO spectroscopic archive provides excellent opportunities to examine the distributions of various spectral lines. The dynamical, physical, and chemical properties of the galaxies can be studied using these spectroscopic data. In the near infrared, there are many emission lines produced by various mechanisms. Since different lines are formed under different conditions, the comparison of several different lines in different locations within the galaxy provides useful information regarding the physical and chemical status of the galaxy.

In this paper, we analyze the infrared spectra from the nearby starburst galaxy, M82, which was intensively observed by many methods, including ISO. M82 (NGC3034, Arp337) is a nearby (3.25 Mpc, Tammann & Sandage 1968) archetypical starburst galaxy (Rieke et al. 1993). Since the inclination of the galaxy is about 80° (Schreiber 1999), it is observed as edge-on. The luminosity of the far-infrared continuum within the central 1′ region (corresponding to 950 pc) is ~2.8×10^{10} $L_\odot$, and the integrated luminosity of the [CII] 158 μm line is ~5.0×10^{7} $L_\odot$ (Stacey et al. 1991). M82 is close enough to study the central regions, where the star formation is very active.

This paper is organized as follows. In Section II we show the collected data from the archive. In Section III we describe the reduction method. We present the results from the data reduction and line identifications in Section IV. Finally, we summarize our results in Section V.

II. OBSERVATIONAL DATA

M82 (α_{2000}=09^h 55^m 52^s.40, δ_{2000}=+69° 40′ 47.″0) was observed with the ISO Short Wavelength Spectrometer (SWS, De Graauw et al. 1996; Schaeidt et al. 1996) at 11 positions along the major axis including the nucleus.

The observed points are separated by $\Delta\alpha$=1^s.6 and $\Delta\delta$ = 3″.4 toward the north-east and south-west directions. Thus the angular separation between two adjacent points is 9.″0 (corresponding to 142 pc). In total, the

Table 1. The observing log for M82

Position (")	R.A. (Epoch2000) (h m s)	Dec. (Epoch2000) (° ' ")	Exposure time (sec)
NE 45	09 56 00.30	+69 41 03.9	920
NE 36	09 55 58.70	+69 41 00.5	920
NE 27	09 55 57.10	+69 40 57.1	920
NE 18	09 55 55.50	+69 40 53.7	818
NE 9	09 55 53.90	+69 40 50.4	818
Nucleus	09 55 52.40	+69 40 47.0	818
SW 9	09 55 50.70	+69 40 43.6	818
SW 18	09 55 49.10	+69 40 40.3	818
SW 27	09 55 47.50	+69 40 36.9	920
SW 36	09 55 45.90	+69 40 33.5	920
SW 45	09 50 44.30	+69 40 30.1	920

observations cover about 700 pc from the nucleus along the major axis. Table 1 shows the observing log of M82.

Among many identified spectral emission lines, we have chosen 4 strong ones of different origin, i.e., [ArIII] 8.99 μm, H_2 17.034 μm, [FeII] 25.98 μm, and [SiII] 34.815 μm. All the lines were taken in the grating mode.

The H_2 emission originates from the shocked regions or photodissociation regions (PDRs: Schreiber 1999). The [FeII] 25.98 μm line is from shocked regions. The [ArIII] 8.99 μm line is from HII regions in lower ionization states. The far-infrared (FIR) emission is produced in shocks (Hollenbach & McKee 1989), PDRs, and HII regions (Rubin et al. 1988). Most of the [SiII] 34.815 μm emission comes from PDRs or HII regions Spinoglio & Malkan 1992, (Lord et al. 1996).

III. DATA REDUCTION

We used a post-pipe-line analysis, ISO Spectral Analysis Package (ISAP) Version 6.1a to reduce the data. The archival data are the auto analysis results (AAR) version, and we relied on the basic reduction procedures through the pipeline. At first, data points from cosmic rays are taken out. About 20% of the data was removed by this process as bad data. From the SWS02 Astronomical Observation Template (AOT) data of M82, we

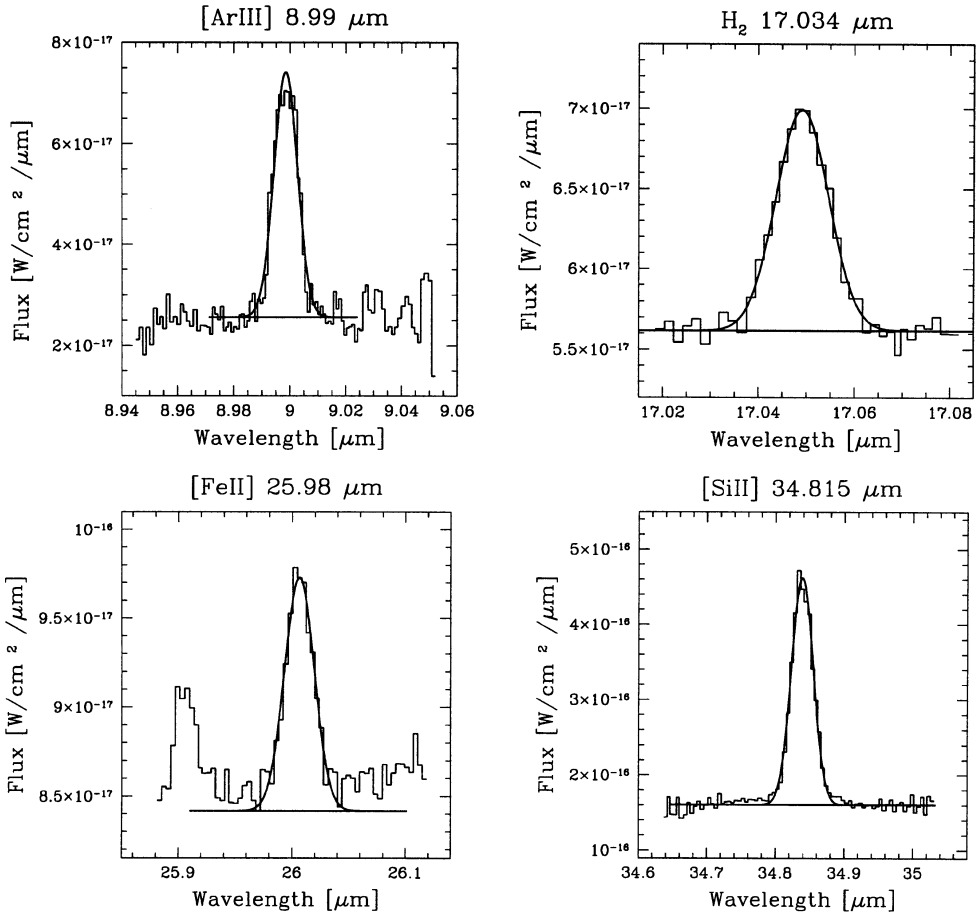

Fig. 1. Examples of Gaussian fitting to the observed lines. All the lines come from the center of M82. The line in the left hand of [FeII] is identified as HeII 25.899 μm.

have chosen four strong emission lines, i.e., [ArIII] 8.99 μm, H_2 17.034 μm, [FeII] 25.98 μm, and [SiII] 34.815 μm. The raw data still has some points that deviate significantly from the majority. Thus we accept data within 2.5 σ range from the median, where σ is the standard deviation defined as,

$$\sigma = \left[\frac{\sum (flux_i - flux_{median})^2}{N(N-1)}\right]^{1/2}, \quad (1)$$

where N is the data points, when N>1. The spectroscopic measurements were done in two scans within the given band: from short to long wavelength and vice versa. There were no significant differences for the results from different directions of the scanning, so the results of both scan directions are averaged.

Since most of the lines are well represented by Gaussian profiles (Valentijn et al. 1996), we fitted the line profiles to a Gaussian function and obtained λ_o, $\Delta\lambda$ and F, where λ_o is the wavelength of the line center, $\Delta\lambda$ is the full width at half maximum (FWHM) and F is the integrated flux of the line. Some examples of the observed profiles and fitted profiles are shown in Fig. 1. In some cases, a double Gaussian gives a better fit to the observed lines, but the second component is usually very weak. Therefore, we did not attempt to fit to multiple components. The line widths obtained here are not the intrinsic line widths because the instruments contribute to the broadening of the lines. We obtain intrinsic line widths by deconvolving the instrumental profiles. This procedure is described in more detail in Section IV. (c).

IV. RESULTS

(a) Flux Distribution

Table 2 shows the fluxes of our selected lines at the observed locations. In Fig. 2, we show the integrated and normalized flux distributions of these four lines against their positions. To obtain the integrated flux, we used the best-fitting Gaussian profiles in order to avoid any ambiguity arising from noise. The integrated flux distributions of the emission reflect the status of the gases at the observed positions.

All the line flux distributions have a nearly symmetrical shape along the major axis. The [ArIII] 8.99 μm, [FeII] 25.98 μm, and [SiII] 34.815 μm lines, which originate from HII regions, show symmetrical shapes with peaks located near the nucleus. However, the H_2 17.034 μm emission has twin peaks at about 200 pc from the center. This "twin peaks" phenomenon of molecular emission is a common occurrence in starburst or barred galaxies.

The H_2 emission is coming from broader regions than the other lines. Previous studies of the center of M82 show an elongated structure of ~200 pc ×400 pc (Joy, Lester & Harvey 1987; Telesco & Gezari 1992; Waller, Geweell & Tamura 1992). Some observations of HI (21 cm) emission (Weliachew, Formalont & Greisen 1984) and 30 μm dust emission (Telesco et al. 1991) show dual peaks at distances of 75-225 pc from the center along the major axis. The origin of the twin peaks is thought to be related to the orbit crowding of molecular clouds near the Inner Lindblad Resonances (ILR) (Kenney et al. 1992; Telesco & Decher 1988; Larkin et al. 1994; Lord et al. 1996). Alternatively, it is from the tightly wrapped inner spiral arm (Telesco et al. 1991; Shen & Lo 1995). The molecular cloud or wrapped spiral arm starts at ~125 pc from the nucleus (Loiseau et al. 1990). The starburst regions are concentrated within the rotational rings which are located at the outer edge of the bar or at around 200 pc from the nucleus (Telesco et al. 1991). H_2 emission appears to be associated with the rotational rings at ~200 pc just outside the inner spiral arm.

The relative depletion of the H_2 emission in the central region may reflect the fact that most of the molecules are dissociated in the region where star formation is very active. The central part of M82 is characterized by a strong radiation field (Colbert et al. 1999), which effectively dissociates the H_2 molecules.

Table 2. The Flux Values of the Emission Lines from M82

Position (arcsec)	[ArIII][a] 8.99 μm	H_2[a] 17.034 μm	[FeII][a] 25.98 μm	[SiII][a] 34.815 μm
NE 45	...	0.57	0.18	5.33
NE 36	...	0.93	0.29	11.4
NE 27		1.7	1.0	26.8
NE 18	1.26	2.16	1.55	51.8
NE 9	2.87	1.92	2.49	90.9
Nucleus	5.14[b]	1.87	3.24	118
SW 9	5.07	2.04	3.55	103
SW 18	3.07	2.09	2.55	69.7
SW 27	1.36	1.75	1.37	35.4
SW 36		1.27	0.57	16.0
SW 45		0.85	0.23	6.01

[a]The flux values in units of 10^{-19} W cm^{-2}.
[b]Schreiber (1999) presented the flux of [ArIII] 8.99 μm as 4.89×10^{-19} W cm^{-2} from the ISO SWSO1 data.

(b) Rotational Velocity Distribution

Since M82 is a nearly edge-on galaxy, we can observe the rotational velocity along the major axis. We show the distribution of V_{LSR} obtained from fitting the lines to Gaussian profiles in Fig. 2. Also shown in this

figure is the rotation curve obtained by using the SIII 9069 Å line by Mckeith et al. (1993). The near IR SIII line has a resolution of ~1″ but ISO has much larger beam size (14″×20″). The slow rise of the lines in the present study is due to the large beam size. The peak rotation velocity is also affected by the resolution. The ISO spectra shows a smaller peak velocity than the SIII 9069 Å observations.

(c) Velocity Dispersion

The FWHM of spectral lines contains information on the kinematics of the components from which the lines originate. However, the ISO spectrometers have relatively broad instrumental profiles. In order to obtain intrinsic profiles, we have to remove the instrumental effects. The instrumental line profiles of the ISO grating can be approximated by a Gaussian (Valentijn et al. 1996).

Suppose that the intrinsic line profile of the object is a Gaussian profile with line width γ,

$$i(\lambda') = C_1 e^{-(\lambda-\lambda_o)^2/\gamma^2} \quad (2)$$

where λ_0 is the wavelength of the line center. Also suppose that the response of the spectrometer is another Gaussian broadening function with width Γ_1,

$$\phi(\lambda, \lambda') = C_2 e^{-(\lambda'-\lambda)^2/\Gamma_1^2} \quad (3)$$

where λ is the wavelength of the incoming photons. Then, the observed profile is a result of the convolution of the intrinsic profile and the instrumental response function, i.e.,

$$I(\lambda) = \int_0^\infty i(\lambda')\phi(\lambda, \lambda')\mathrm{d}\lambda'$$

$$= C_2 \int_0^\infty i(\lambda') e^{-(\lambda-\lambda')^2/\Gamma_1^2} d\lambda' \quad (4a)$$

$$= C_1 C_2 C_3 \, e^{-\frac{1}{\gamma^2+\Gamma_1^2}(\lambda-\lambda_o)^2}, \quad (4b)$$

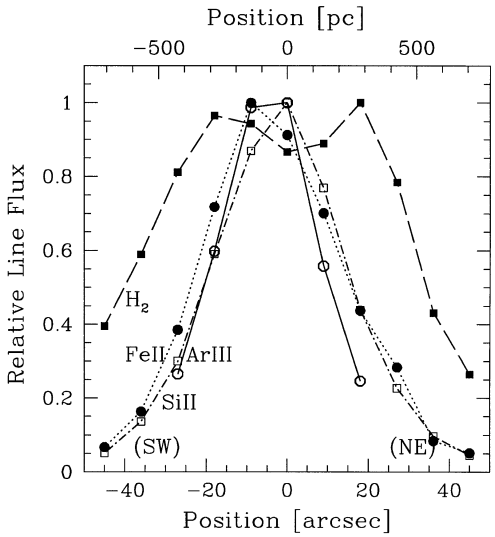

Fig. 2. The flux distributions of [ArIII] 8.99 μm, H_2 17.034 μm, [FeII] 25.98 μm, and [SiII] 34.815 μm emissions along the major axis of M82. The integrated fluxes were obtained by integrating the best fitted Gaussian profiles. The flux scales were normalized to the peak values.

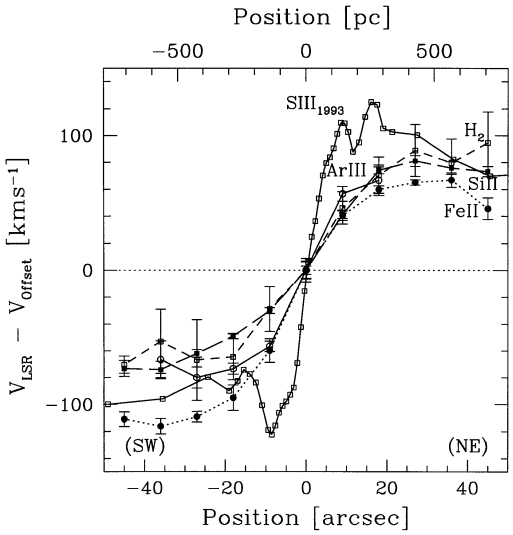

Fig. 3. The V_{LSR} distributions of [ArIII] 8.99 μm, H_2 17.034 μm, [FeII] 25.98 μm, and [SiII] 34.815 μm emissions along the major axis of M82. V_{LSR} was obtained from the Gaussian fitting to the observed lines.

Table 3. The characteristics of each wave band in the SWS AOT

Emission Line	Wavelength [μm]	Band	Spectral Resolving Power (R=λ/Δλ)[a]	Velocity Resolving Power (km s^{-1})	Estimated Resolving Power from Orion (km s^{-1})
[ArIII]	8.99	2C	1680	178.57	
H_2	17.03	3C	1825	164.38	150.88
[FeII]	25.99	3D	1140	263.16	213.27
[SiII]	34.81	4	1200	250.00	213.59

The R values are obtained by observing an extended source (the ISO observation Manual, 1996).

Table 4. The velocity dispersion from the observed emissions

Position (arcsec)	[ArIII]		H_2		[FeII]		[SiII]	
	σ_{obs}	σ_{int}	σ_{obs}	σ_{int}	σ_{obs}	σ_{obs}	σ_{obs}	σ_{int}
	(km s^{-1})		(km s^{-1})		(km s^{-1})		(km s^{-1})	
NE 45	...	...	184.51	34.92	259.53			
NE 36	...	...	193.61	42.63	253.27			
NE 27	...	...	196.34	44.74	303.97	63.39	274.51	47.24
NE 18	214.71	49.67	197.50	45.62	2888.6	49.38	278.56	51.19
NE 9	281.82	90.84	196.43	44.81	290.30	51.06	334.81	92.80
Nucleus	328.3	114.83	236.50	70.85	355.01	99.28	326.37	87.42
SW 9	258.13	77.66	234.27	69.55	305.01	64.25	288.31	59.83
SW 18	186.89	22.98	210.30	54.65	226.88	...	253.09	16.44
SW 27	177.261	...	189.74	39.49	294.61	55.19	234.31	...
SW 36	113.601	...	187.59	37.66	260.19	...	230.28	...
SW 45	198.77	46.56	230.11	...	238.01			

where

$$C_3 = \int_0^\infty e^{-\left(\frac{1}{\gamma^2}+\frac{1}{\Gamma_1^2}\right)\left(\lambda' - \frac{\Gamma_1\lambda_o + \Delta\lambda}{\gamma^2+\Gamma_1^2}\right)^2} d\lambda = \left(\frac{\pi}{\gamma^2+\Gamma_1^2}\right)^{1/2}. \quad (5)$$

Therefore the convolved line will have a Gaussian profile with width Γ defined by

$$\Gamma^2 = \gamma^2 + \Gamma_1^2. \quad (6)$$

The line width Γ is related to the FWHM by $\Delta\lambda = \Gamma(\ln 2)^{1/2}$. The instrumental line width Γ_1 is given in the ISO SWS Observer's Manual as a function of wavelength and band for an extended source. This Γ_1 is measured by laser in the laboratory. The instrumental profile can also be determined by the observed lines with very narrow intrinsic width.

In order to check the validity of the laboratory data, we have analyzed the spectral lines toward the Orion region, where the intrinsic line widths are expected to be very small. From the ISO archive, we have selected SWS02 data in the same mode as the M82 data, from Orion PK1 and Orion Brga, and identified HeII 7.457 μm, H_2 8.04 μm, H_2 9.66 μm, [ArIII] 8.99 μm, H_2 17.034 μm, [FeIII] 22.9 μm, [FeII] 25.98 μm, and [SiII] 34.815 μm lines. The intrinsic widths of these lines are of order of 1~10 km s^{-1}, which is much smaller than the instrumental width of ~100 km s^{-1}. Therefore, we may assume the broadening of these lines is purely due to instrumental effects.

We have checked these values with the emission lines from Orion. We obtained the $\Delta\lambda$ from the single Gaussian line fitting. Since the intrinsic widths of these data are much smaller than the instrumental widths, we can assume that $\Delta\lambda_{orion} = \Delta\lambda_{instrument}$. Table 3 shows the comparison of the characteristics of the instrument from the laboratory measurements and the results from Orion.

The instrumental resolutions are strictly applicable to the extended sources only. For the SW band, instrument profiles of the point source are estimated to be about a factor of 2 narrower. However, the LW resolution is not affected by the size of the source. The results from Orion are plotted in Fig. 4 along with the laboratory values (Valentijn et al. 1996) for all bands which are used in this study. The Orion observations may not exactly be extended sources. For the deconvolution of M82, we simply used the laboratory measurement rather

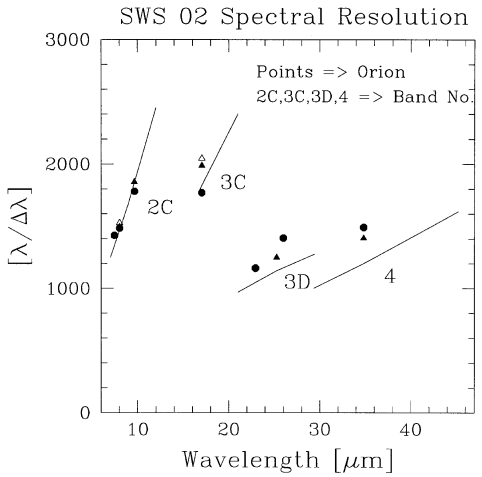

Fig. 4. The comparison between the spectral resolution of the SWS manual (solid lines) and that of the results from Orion (plots). The filled circles indicate the results from Bar Brga region and the open and filled triangles are from the PK1 in Orion with slightly different positions.

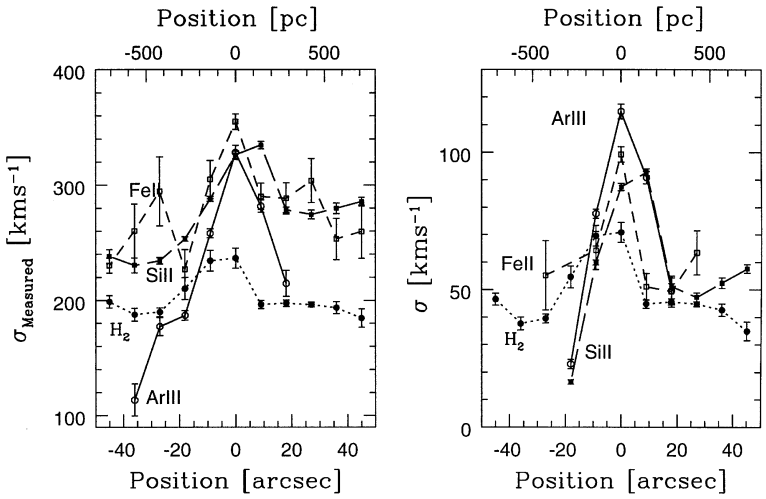

Fig 5. The FWHM distributions of the observed profiles (left panel) and the deconvolved profiles (right panel) in M82. The FWHM values of the deconvolved profiles are substantially less than those of the observed profiles. At the outer parts, σ is ~50 km s^{-1}. The very small dispersion of [SiII] and [ArIII] at the negative positions may be due to the large uncertainties at the estimates of line widths and nearly comparable widths between the instrumental and the observed profiles. The large velocity dispersion in the central region is mostly due to the rotation within the resolution.

than the Orion results since not all the spectral lines were available for Orion.

In Table 4 and Fig. 5, we show the measured and intrinsic velocity depletion after the decon-volutions. All lines show a higher velocity dispersions at the center and a gradual decrease outward along major axis. Also note that the intrinsic velocity dispersions for different lines are different. The [ArIII] line shows the highest central dispersion (~120 km s^{-1}) and the H_2 line shows the lowest one (~70 km s^{-1}). Outside the nuclear region, the velocity dispersions of all lines are nearly the same at ~50 km s^{-1}.

Of our selected lines, only [ArIII] belongs to the SW band. Therefore, the large velocity dispersion of the [ArIII] line can not be due to the underestimation of the instrumental line width. From Fig. 5, we can safely assume that the H_2 line is coming from the extended region, but the emitting regions of the other lines could be somewhat smaller than the size of the beam. Our estimates of [SiII] and [FeII] lines should be valid. We clearly see the rapid increase in velocity dispersion of most of the lines toward the central region. The large velocity dispersion in the central region is partly caused by the rotation within the beam.

The rotation velocity rises to ~100 km s^{-1} within ~5″ from the center. Therefore we may expect that the central velocity dispersion for any line will be strongly affected when observed with ~10″ resolution. However, it is not clear why different lines show significantly different central velocity dispersion. H_2 has the lowest dispersion of ~70 km s^{-1} and [ArIII] has the higest dispersion of ~120 km s^{-1}. The H_2 line has a rather extended dispersion with a relative depletion in the center. Therefore this line may not have been significantly affected by the central rotation. Also if H_2 molecular emission mostly comes from 200 pc molecular ring, we expect relatively small velocity dispersion. [ArIII] is the only line whose instrumental profile depends on the nature of the source. The instrumental profile may be even narrower than our chosen width, and the intrinsic width of this line may be broader. Generally speaking, the velocity dispersion of the gas is smaller than that of the stars because the random velocity component among the clouds can be easily dissipated through hydrodynamical collisions. The large central velocity distribution of [ArIII] needs further confirmation, since it seems to contradict to the other data.

(d) Position-Velocity Diagrams

One of the most powerful methods to trace the kinematics of the central parts of galaxies is to use the position-velocity diagrams. Using ISO data, we have generated position-velocity diagrams for [ArIII], H_2, [FeII] and [SiII] as shown in Fig. 6. We have used the observed profiles in obtaining these diagrams. We can see the diverse features of the gas kinematics from this figure as expected from the rather diverse distribution of the flux and line width. The [ArIII] line shows a rather asymmetric distribution, as was evident from Fig. 2. The double peaked nature of H_2 is clearly seen. Since these peaks have opposite velocity, they are clearly originating from a ring structure. In the [FeII] position velocity map, we have one more anomaly in the lower-

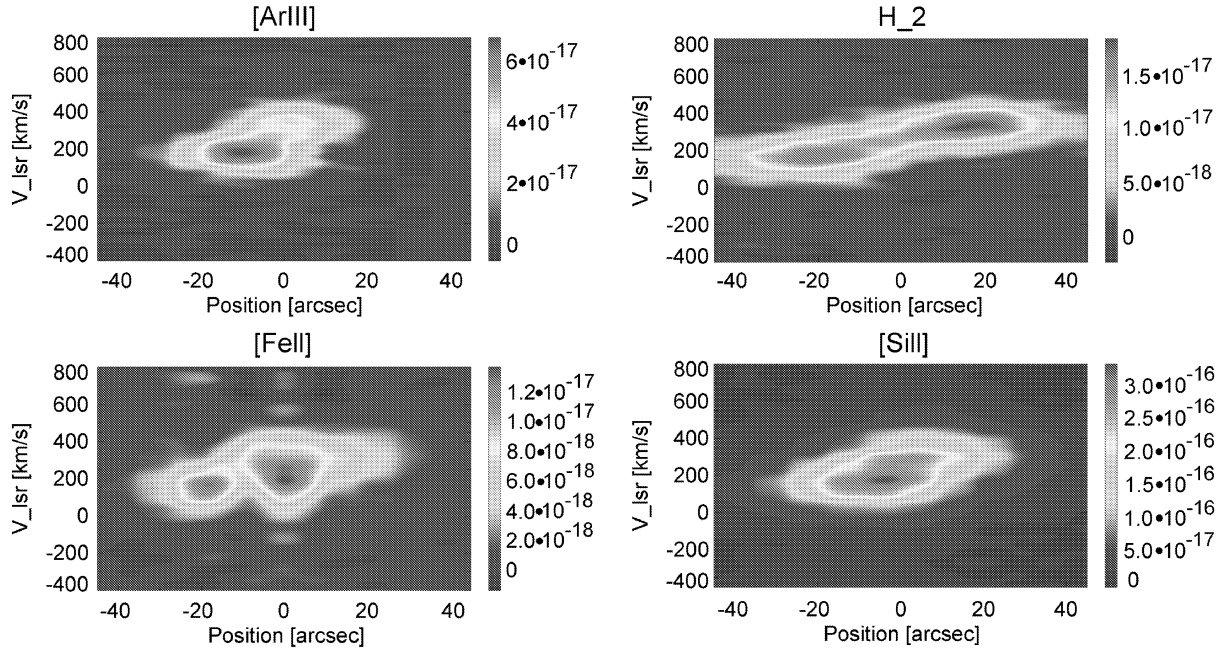

Fig. 6. The position-velocity diagrams of four lines in the present study. in lower left area of the [FeII] line is due to HeII 25.899 μm line.

left area: this is simply due to the HeII 25.899 μm line. For this [SiII] line, there is an extended component at positive 9″ and ≈400 km s^{-1}. Similar feature was observed by Lord et al. (1996) at the center of M82 with the same line observed by the Kuiper Airborne Observatory (KAO).

V. SUMMARY

The goals of this paper were to compare the infrared line emission from various regions in M82. We analyzed ISO SWS02 data for M82 in which the active central regions emit [ArIII] 8.99 μm, [FeII] 25.98 μm, and [SiII] 34.815 μm lines. These lines have different origins and they show different distributions. H_2 molecular emission has a relatively broad distribution near the nucleus of M82. The intensity profile of the twin peaks is located at ~200 pc from the center, indicating the presence of rotating molecular clouds. Other lines are highly concentrated toward the central regions.

The Observed line profiles are fitted by Gaussians and we have removed the instrumental broadening by deconvolution under the assumption that the instrumental profiles are also Gaussian. We have checked the laboratory measurements of the width of the instrumental profiles by analyzing the selected line profiles towards the Orion cloud. We found that the observed profiles agree with the laboratory measurements to within ~20%. The velocity dispersion obtained by the deconvolution is found to be ~50 km s^{-1} outside the nucleus. The dispersion at the nucleus become larger than ~100 km s^{-1}, due to significant contribution from the rotation because of the larger beam size. We have generated position-velocity diagrams for the lines that we have analyzed. All four lines show significantly different morphologies in these diagrams. [SiII] and [ArIII] clearly show the extended features outside the nucleus. This is thought to be due to the HII regions located at ~12″ from the nucleus. The H_2 molecular line shows a clear double peak at ±20″, implying a rotating ring.

This work was financially supported by the BK21 project of the Korean Government and by KOSEF through grant 1999-2-113-001-5. JS acknowledges the organizers of ISO Summer School in 1998 for the financial support to attend.

REFERENCES

Colbert, J. M. et al. 1999, ApJ, 511, 721
De Graauw, Th. et al. 1996, AA, 315, L49
Hollenbach, D. J., & McKee, C. F. 1989, ApJ, 342, 306
Joy, M., Lester, D. F., & Harvey, P. M. 1987, ApJ, 319, 314
Kenney, J. D. P., Wilson, C. D., Scoville, N. Z., Devereux, N. A., & Young, J. S. 1992, ApJ, 395, L79
Kessler, M. F., Steinz, J. A., Anderegg, M. E., Clavel, J., Drechsel, G., Faelker, J., Riedinger, J. R., Robson, A., Taylor, B. G., & de Ferrián S. X. 1996, AA, 315, L27
Leech, K., de Graauw, T., van der Hucht, K. A., & Lutz, D. 1996, ISO Short Wavelength Spectrometer Observer's Manual, Issue 3.0
Loiseau, N., Nakai, N., Sofue, Y., Wielebinski, R., Reuter,

H. P., & Klein, U. 1990, AA, 228, 331
Larkin, J. E., Graham, J. R., Matthews, K., Soifer, B. T., Beckwith, S., Herbst, T. M., & Quilen, A. C. 1994, ApJ, 420, 592
Lord, S. D., Hollenbach, D. J., Haas, M. R., Rubin, R. H., Colgan, S. W. J., & Erickson, E. F. 1996, ApJ, 465, 703
McKeith, C. D., Castles, J., Greve, A., & Downes, D. 1993, AA, 272, 98
Rieke, G. H., Liken, K., Rieke, M. J., & Tabellen, P. 1993, ApJ, 412, 99
Rubin, R. H., Simpson, J. P., Erickson, E. F., & Haas, M. R. 1988, ApJ, 327, 377
Schaeidt, S. G. Morris, P.W., Salama, A., Vaudenbussche, B., Beintema, D. A., Boxhoorn, D. R., Feuchtgruber, H., Heras, A. M., Lahuis, F., Leech, K., Roelfsema, P. R., Valentijn, E. A., Bauer, O. H., van der Bliek, N. S., Cohen, M., de Graauw, Th., Haser, L. N., van der Hucht, K. A., Huygen, E., Katterloher, R. O., Kessler, M. F., Koornneef, J., Luinge, W., Lutz, D., Planck, M., Spoon, H., Waelkens, C., Waters, L. B. F. M., Wieprec ht, E., Wildeman, K. J., Young, E., & Zaal, P., 1996, AA, 315, L55.
Schreiber, N. M.,1999, ApJ, 373, 423S Ph. D. Dissertation, LMU in Munich
Shen, J., & Lo, K. Y. 1995, ApJ, 445, L99
Spinoglio, L. & Malkan, M. A., 1992, ApJ. 339, 504
Stacy, G. J., Geis, N., Genzel, R., Lugten, J. B., Poglitsch, A., Sternberg, A., & Townes, C. H., 1991, ApJ, 373, 423S
Tammann, G. A. & Sandage, A. 1968, ApJ, 151, 825
Telesco, C. M., Campins, H., Joy, M., Diets, K., Decher, R. 1991, ApJ, 369, 135
Telesco, C. M. & Decher, R. 1988, ApJ, 334, 573
Telesco, C. M. & Gezari, D. Y. 1992, ApJ, 395, 461
Tielens, A. G. G. M. & Hollenbach, D. 1985, ApJ, 291, 722
Valentijn, E. A., Feuchtgruber, H., Kester, D. J. M., Roelfsema, P. R., Barr, P., Bauer, O. H., Beintema, D. A., Boxhoorn, D. R., de Graauw, Th., Haser, L. N., Heske, A., Heras, A. M., Katterloher, R. O., Lahuis, F., Lutz, D., Leech, K. J., Morris, P. W., Salama, A., Schaeidt, S. G., Spoon, H. W. W., Vandenbussche, B., Wieprecht, E., Luinge, W., & Wildeman, K. J. 1996, AA, 315, L60
Waller, W. H., Gurwell, M., & Tamura, M. 1992, AJ, 104, 63
Weliachew, L., Fomalont, E. B., Greisen, E. W. 1984, AA, 137, 335